

## Modeling on convective boiling heat transfer in a microtube based on flow visualization

Tzu-Hsiang Yen, Yuji Suzuki and Nobuhide Kasagi

Department of Mechanical Engineering, The University of Tokyo, Bunkyo-ku, Hongo 7-3-1, Tokyo, 113-8656, Japan

**Keywords :** Convective boiling, Flow visualization, Microchannel, Periodic flow pattern variation

### 1. INTRODUCTION

Convective boiling heat transfer in microchannels has become an important issue since its high potential on electronic device cooling, highly efficient compact heat exchangers and the reformers for fuel cells.

Recently, many research works focusing on boiling heat transfer in mini or micro channels have been carried out and peculiar heat transfer characteristics have been discovered and discussed. Ravigururajan (1998) measured the average heat transfer coefficient in parallel microchannels of 425 $\mu\text{m}$  ID. Saitoh et al. (2000) employed 1.12 and 0.51 mm ID tubes with R-134a refrigerant, offer the local heat transfer coefficient data. Yen et al. (2003) measured the local heat transfer coefficients in single SUS 304 microtubes from 0.19~0.51 mm ID. Kandlikar (2004) measured the average heat transfer coefficients in parallel microchannels of 200  $\mu\text{m}$  ID. All the above experimental results above show the similar tendency: The heat transfer coefficient decreases with increasing vapor quality and very small dependence of the heat transfer coefficient to heat and mass fluxes at low heat and mass fluxes.

On the other hand, many visualization researches focusing on explanation of the above peculiar heat transfer characteristics have been carried. Steinke et al. (2003) conducted a series of saturated convective boiling experiments in SUS304 parallel microchannels of 214 $\mu\text{m}$  width, 200 $\mu\text{m}$  depth and 57.15mm long. They found that flow patterns in microchannels are similar to those in conventional channels. As to the adiabatic two-phase flows in microchannels, Serizawa et al. (2002) carried out the visualization experiments of adiabatic air-water two-phase flow experiments in single circular capillaries of 20, 25 and 100  $\mu\text{m}$  ID. They made the two-phase flow pattern transition map according to the experimental results and found that the flow map has similar trends of that by Mandhane et al. (1974) for conventional tubes. Moreover, Thomas et al. (2003)

investigated the flow pattern characteristics of adiabatic two-phase flow in etched silicon microchannels of ID 200 $\mu\text{m}$  and 800  $\mu\text{m}$ . It is also conjectured that the flow maps for different of channels are similar.

Such contradiction of the similarity in flow patterns but dissimilarity in heat transfer characteristics between micro and conventional channels shows that there still exist unknown physical mechanisms, which may be dominant to the peculiar heat transfer characteristics.

Therefore, the present study aims at carrying out visualization of liquid superheat and convective boiling with the simultaneous measurement of the local heat transfer coefficient and pressure loss in a circular microtube in order to avoid the effect of interaction of channels in multi-microchannels. Finally, a heat transfer model based on empirical correlations should be established for engineering applications.

### 2. EXPERIMENTAL SETUP FOR VISUALIZATION

Figure 1 shows the flow loop and the test section used in the present experiments. Three different refrigerants: HCFC123, FC72 and ethanol were employed as a working fluid. A twin plunge pump (Moleh, MT-2221) was employed in most experiments in order to provide mass flux from 50 to 350  $\text{kg}/\text{m}^2\text{s}$ . Unlike a single plunge pump, the twin plunge pump keeps a constant flow rate without introducing unwanted bubbles into the test section. The uncertainty interval of the flow rate is within  $\pm 1\%$ . The working fluid was heated with a secondary water loop at the inlet, and its temperature was kept at 10 K below the saturated temperature.

Figure 2 shows the test section used in the present experiment. A Pyrex glass tube, which was 0.3 mm in inner diameter and 0.5 mm in outer diameter, was applied. The tolerance of the inner and outer diameters was  $\pm 20\mu\text{m}$  and  $\pm 15\mu\text{m}$ , respectively. In order to heat the tube, the mixture of ITO (Indium Tin Oxide) and silver was evenly sputtered on the

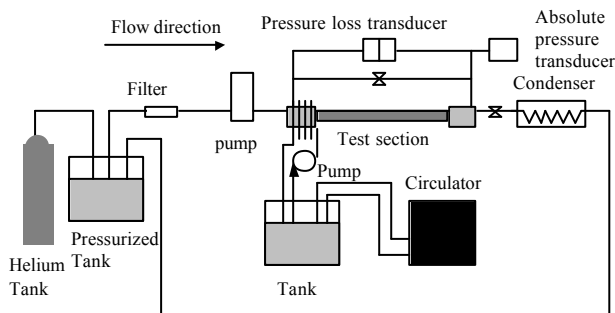


Fig. 1 Experimental loop

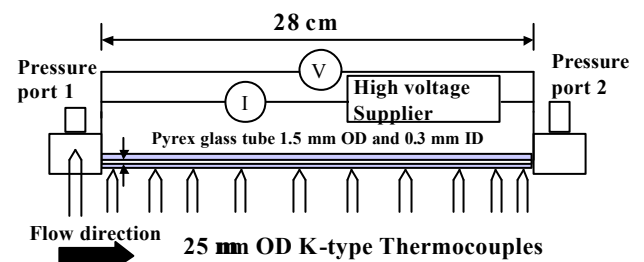


Fig. 2 Test section

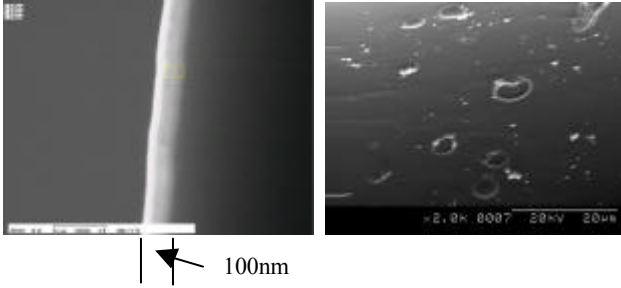


Fig. 3 SEM photos of the 0.3 mm ID Pyrex glass micro tube. Left: 100 nm ITO/Ag sputtering film. Right: Inner surface condition

outer surface of the tube. The sputtered film thickness was about 100nm, as shown in the left side of fig. 3. The total resistance of the sputtered glass tube was about 1000 Ω. Twelve K-type thermocouples of 25 μm OD, calibrated with the accuracy of ±0.05 K, were glued on the tube outer surface with thermally conductive silicon.

The left photo in fig 3 shows the SEM images of inner surface of of 0.3 mm Pyrex glass tube. Although some shallow cavities having diameters around 5 μm are sparsely distributed, the effective cavity for nucleate boiling is considered to be the edge of these large but shallow cavities. These edges are usually 1~2 μm in width. Smaller cavities with about 2 μm in diameter are also observed.

A high-speed CMOS camera (Vision Research, Phantom v7) was employed for the flow visualization. The images having 800x100 pixels were taken at 20000 frames/sec.

### 3. DATA REDUCTION

The data reduction method is based on the method by Yen et al. (2003). First of all, a preliminary heating experiment with keeping the test section empty is carried out in order to estimate the heat loss to the air. Then the inner wall temperature can be solved though the one-dimensional heat conduction equation in the cylindrical coordinates, i.e.,

$$T_{win} = T_{wmiddleglass} - \frac{\ln\left(\frac{D_o}{D_i}\right)q(x)D_i}{2k}, \quad (1)$$

where  $T_{wmiddleglass}$  represents the temperature on the inner side of the deposition layer, which can be calculated through another one-dimensional heat conduction equation with heat generation as shown in Yen et al. (2003).

Finally, the heat transfer coefficient is calculated as:

$$h(x) = \frac{q}{T_{win}(x) - T_{ref}(x)}, \quad (2)$$

where  $T_{ref}(x)$  is the local bulk mean temperature of the refrigerant. When the fluid is in the saturated region, the local bulk mean temperature is equal to the saturation temperature, and is derived from the local pressure distribution  $P_{sat}(x)$ .

The local pressure  $P_{sat}(x)$  in the saturated boiling region is assumed to be linearly distributed along the tube, and given by

$$P_{sat}(x) = P_{sat}(l) - \Delta P_{sat} \frac{x-l}{s}. \quad (3)$$

After the pressure loss of the test section reaches the steady state, the wall temperature shows some quasi-periodic variation in the saturated boiling conditions. The temperature amplitude is about 1.5 K. The average wall temperature is obtained by the ensemble averaging over 30 minutes.

As the same as Yen et al. (2003), the propagation of the componential uncertainties in data reduction error is estimated by ANSI/ASME PTC 19.1 through the data reduction method described above. The uncertainty interval of the inner wall temperature is about 0.2 and the final uncertainties for the heat transfer coefficients are still within ±10%.

## 3. EXPERIMENTAL RESULTS

### 3.1 Visualization in the microtube

In order to understand the relationship between heat transfer characteristics and their corresponding physical mechanism in the flow field, a simultaneous measurement of the local heat transfer coefficient and flow visualization is carried out. According to the visualization experiment at a fixed streamwise position of the Pyrex glass tube with simultaneous measurement of local heat transfer coefficient, the flow pattern varies dramatically in time and exhibits some quasi-periodic variation. The observed flow patterns in such quasi-periodic variation include bubbly, plug, slug and independent droplet flows and the period of such variation is about 0.2 sec. in all experimental runs of this research. The visualization results of these flow patterns are shown in figs. 4 to 7, respectively.

Figure 4 shows the images of bubbly flow pattern. With the aid of high-speed camera, it is observed that the bubbles move in spiral direction downstream with the speed of about 2.6 m/s, as those indicated in the circle marks. Moreover, notice that compared with conventional tubes, bubbles are sparsely distributed because of the lack of nucleation cavities in microtubes, as described in the previous chapter and also by Brereton et al (1998).

The observed bubbles soon extend and become plugs along with the evaporation. Figure 5 shows the high-speed camera images of the plug flow pattern. It is observed that gas plugs move with the speed of about 2.6 m/s, which is similar to that in the bubbly flow pattern, and gradually extends in the streamwise direction, as those indicated in the rectangular marks. When gas plugs extend to some extent, wave generates from thin films between gas plugs and inner wall on the perimeter of the tube and then these waves emerge, forming the slug flow pattern, as shown in Fig. 6.

Finally, as the evaporation continues, the thin film in slug flow pattern becomes thinner and thinner, finally splitting into independent droplets. Figure 7 shows such independent droplet flow pattern. It is observed that as time goes by, the droplets continue to become smaller. When  $t = 0.06$  sec., the strip-shape droplet in  $t = 0$  sec. to  $t = 0.04$  sec. splits into many small circular droplets, as shown in circle marks of Fig. 6. Such droplet movement can only be observed in very large and long tubes and it is named ‘capillary flow pattern’ by Carey (1992). However, independent droplets observed here have completely different

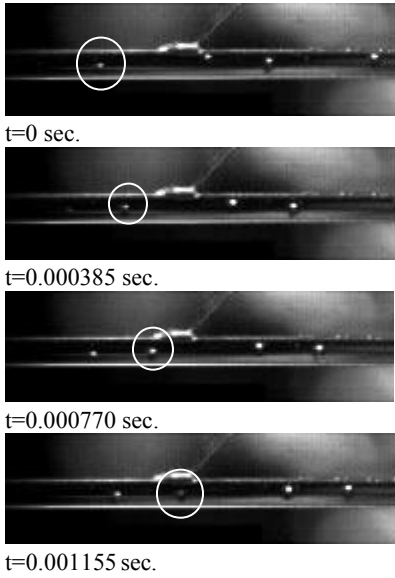


Fig. 4 Bubbly flow pattern in the microtube

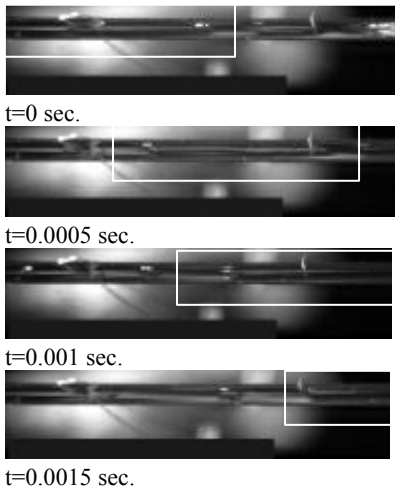


Fig. 5 Plug flow pattern in the microtube

heat transfer characteristics because in microtubes, film thickness of these droplets can be very thin and such thin film thickness always leads to very high heat transfer coefficients.

### 3.2 Comparison of local heat transfer coefficients to their corresponding flow patterns

Figure 8 shows the local heat transfer coefficient versus vapor quality under two different heat fluxes. According to Fig. 8, the local heat transfer coefficient decreases at  $\chi < 0.3$ . When  $\chi > 0.3$ , the heat transfer coefficient becomes almost independent of the vapor quality and seems to be also independent of heat flux. All these heat transfer characteristics are similar to the experimental results in 0.19 and 0.51 mm ID SUS304 tubes by Yen et al. (2003). Fig. 9 shows the local heat transfer coefficient under different mass fluxes. The local heat transfer coefficient seems to be also independent of mass fluxes. Such independence is similar to the experimental results in both microtubes (Yen et al., 2003) and mini-tubes (Bao et al., 2000, Kew et al, 1997).

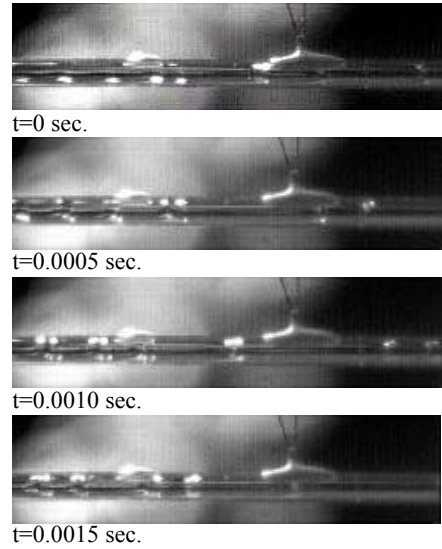


Fig. 6 Slug flow pattern in the microtube

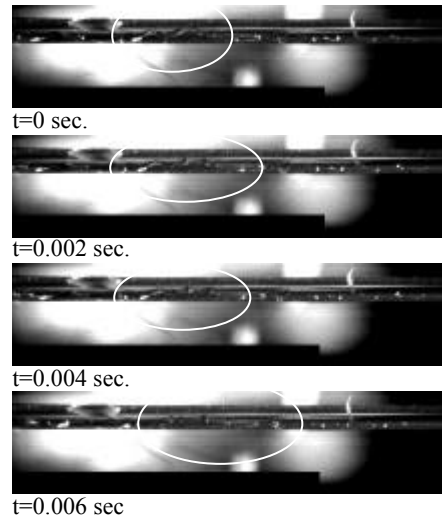


Fig. 7 Independent droplet flow pattern in the microtube

Figure 10 shows the time history of each flow patterns in one period at measuring point of local heat transfer coefficients of each experimental run described in Figs. 8 and 9. Each graph in fig. 10 represents one experimental run. The partial dry-out flow pattern means the independent droplet flow in fig. 7. Time history moves forward along the direction of the arrow on y-axis. From this figure it is observed that periodic variation occurs at every visualization points and the ratio of the plug and slug flow patterns remain similar along the all vapor qualities of the test section, while the ratios of bubbly flow and single phase liquid flow pattern decrease and dry-out region increases. It is also important to notice that the bubbly flow pattern always appears and has about 30% time history of the total period at lower vapor quality ( $\chi < 0.3$ ). Since there are always larger heat transfer coefficients at low vapor quality in both Pyrex glass and other metallic tubes, it is conjectured that the relatively large heat transfer coefficient at low  $\chi$  is due to the existence of the bubble nucleation. On the other hand, the ratio between the

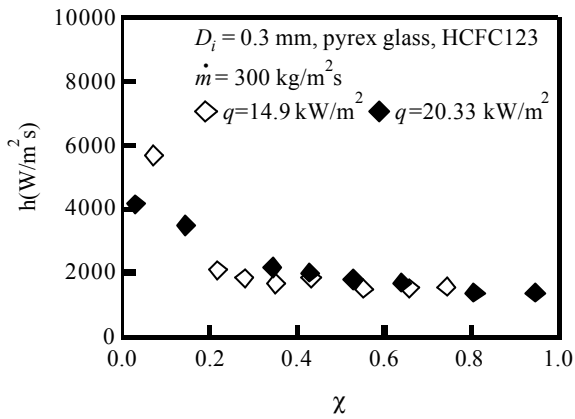


Fig. 8 Local heat transfer coefficients versus vapor quality under different heat fluxes.

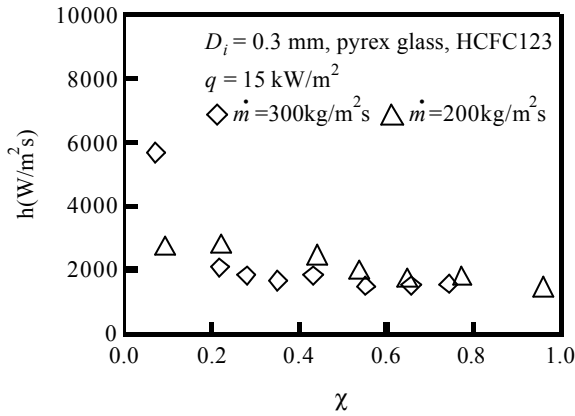


Fig. 9 Local heat transfer coefficients versus vapor quality under different mass fluxes.

plug, slug and annular flow patterns remains the largest ratio and unchanged along all the vapor qualities, so the heat transfer coefficient is almost constant at  $\chi > 0.3$ . Although in the independent droplet flow pattern, droplets are considered to have very high heat transfer coefficients because of the thin film boiling in these droplets, the local heat transfer coefficient remains unchanged at  $\chi > 0.3$ . The minor dominance of the independent droplet flow pattern is because that when the thin film becomes thinner; the partial dry-out area also becomes larger as shown in high-speed camera images of Fig. 11. Finally the heat transfer coefficient over a period of time remains small because of the balance between the very high heat transfer coefficient of thin film and the very low heat transfer coefficient of the dry-out area, where the latter one is much larger than the previous one.

Finally, from the overall comparison of figs. 8 to 10, it is observed that, even in different heat fluxes or mass fluxes, when the local heat transfer coefficients and the vapor quality are similar, the ratios of flow patterns are similar. So in micro tubes, the restriction of bubble growth space also restricts the flow pattern variation in different heat and mass fluxes. The dominant parameter to local heat transfer coefficients becomes the ratio of flow pattern variation and bubble nucleation at lower

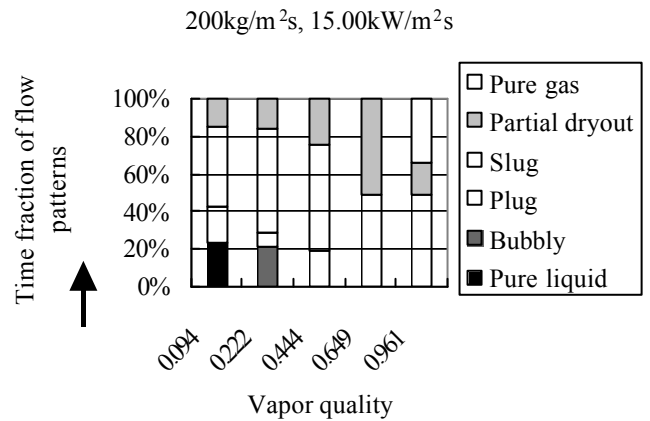
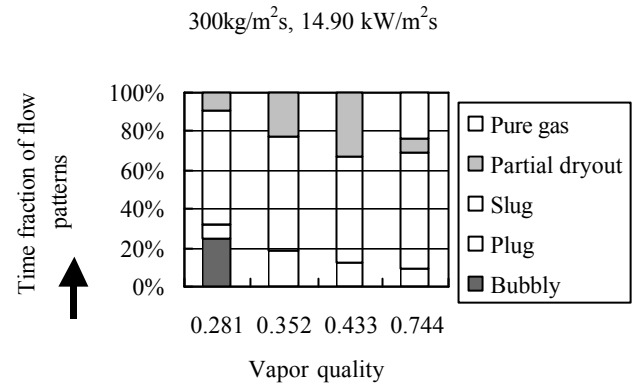
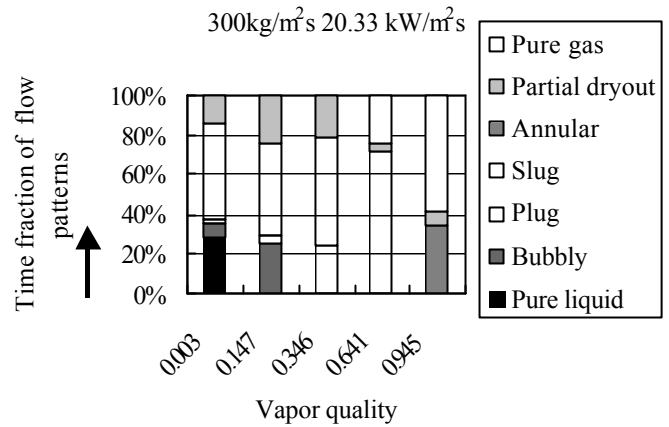


Fig. 10 Distribution of the flow patterns under one period at different visualization points of the test section of three experimental runs corresponding to figs. 8 and 9.

vapor qualities. So the traditional empirical correlations, which is based on the steady state of the flow, obviously cannot predict the heat transfer characteristics and a time-dependent model is needed for the radical variation of different flow patterns in microtubes.

#### 4. THE MODEL ON HEAT TRANSFER

As described in the previous chapter, the periodic variation of flow patterns is observed in the microtube. The above fact means the effect of the time history, which is very important for the convective boiling in microtubes is still not taken into consideration.

In order to reflect the correct physical mechanism observed in chapter 3, a model named time fraction model is developed for the prediction of the local heat transfer coefficients and the pressure loss of the convective boiling in microtubes of the ID varies from 0.19 mm to 0.51 mm at low heat and mass fluxes (1~20 kW/m<sup>2</sup>, 50~300 kg/m<sup>2</sup>s).

The ideal form for the time fraction model can be written as:

$$h = a_1 h_{\text{single}} + a_2 h_{\text{bubbly}} + a_3 h_{\text{plug}} + a_4 h_{\text{slug}} + a_5 h_{\text{annular}} + a_6 h_{\text{capillary}} + a_7 h_{\text{dry-out}} \quad (4)$$

and

$$a_1 + a_2 + a_3 + a_4 + a_5 + a_6 + a_7 = 1 \quad (5)$$

In eqns. (4) and (5), the total heat transfer coefficient is obtained from each heat transfer coefficients of different flow patterns, which are widely known to have completely different heat transfer characteristics. The time fraction factor  $\alpha$  represents the percentage of different flow patterns in one period of variation. However, until now, it is still difficult to completely apply the above equations to predict the local heat transfer coefficient because of the lack of the corresponding research results in detailed heat transfer mechanism of each flow pattern.

Therefore, only a simplified model can be applied:

$$h = a_1 h_{\text{single}} + a_2 h_{\text{bubbly}} + a_3 h_{\text{plug, slug and annular}} + a_4 h_{\text{dry-out}} \quad (6)$$

where

$$a_1 + a_2 + a_3 + a_4 = 1. \quad (7)$$

In Eqn. (6), terms  $h_{\text{single}}$  and  $h_{\text{dryout}}$  are obtained from the Nusselt number of the single-phase liquid laminar flow with uniform wall heat flux.  $h_{\text{bubbly}}$  and  $h_{\text{plug, slug and annular}}$  can be obtained from the nucleation and convective boiling term of the current empirical correlations. Finally,  $h_{\text{dry-out}}$  can be obtained from the single phase gas laminar flow.

After comparing many empirical correlations, we choose the nucleation term Chen (1966) and the convective boiling term is obtained from Guerrieri et al. (1956).

The nucleate boiling term of Chen's correlation, which is used in fig. 7.3, has the following form:

$$h_{NB} = 0.00122 \left[ \frac{k_l^{0.79} c_{pl}^{0.45} \rho_l^{0.49}}{s^{0.5} m^{0.29} h_{lv}^{0.24} \rho_v^{0.24}} \right] (T_w - T_{sat}(P_l))^{0.24} (P_{sat}(T_w) - P_l)^{0.75} S \quad (8)$$

where the physical properties of the liquid and the gas are taken to the power  $n$  and  $n = 0.24 \sim 0.79$ .  $P_{sat}(T_w)$  represents the saturation pressure at the wall temperature and  $T_{sat}(P_l)$  represents the saturation temperature of the local pressure.

As to the convective boiling term, Guerrieri et al. (1956) carried out a serious of experiments in convective boiling of conventional tubes and proposed the following relation based on the fitting of their experimental data:

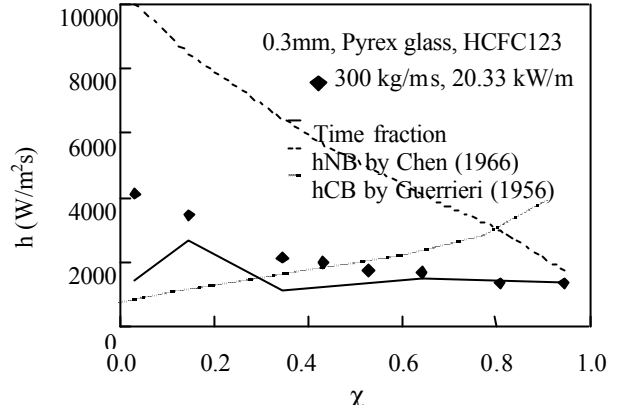


Fig. 11 Comparison of the experimental results and the time fraction model with nucleate boiling term by Chen and convective boiling by Guerrieri et al.

$$\frac{h}{h_1} = 3.4 \left( \frac{1}{X} \right)^{0.45} \quad (9)$$

The parameter  $X$  represents the viscous-viscous or viscous-turbulent Martinelli parameter, which depends on the Reynolds of the liquid and gas, respectively.  $X$  is defined as:

$$X = \left[ \frac{(dP/dz)_l}{(dP/dz)_v} \right]^{1/2} \quad (10)$$

where  $(dP/dz)_l$  and  $(dP/dz)_v$  represent the frictional pressure gradients for the liquid and vapor phases flowing along in the pipe, respectively. These frictional gradients can be computed as:

$$\left( \frac{dP}{dz} \right)_l = - \frac{2f_l G^2 (1-c)^2}{r_l D} \quad (11)$$

$$\left( \frac{dP}{dz} \right)_v = - \frac{2f_v G^2 c^2}{r_v D} \quad (12)$$

$$f_l = B Re_l^{-n}, \quad Re_l = \frac{G(1-c)D}{m_l} \quad (13)$$

$$f_v = B Re_v^{-n}, \quad Re_v = \frac{GcD}{m_v} \quad (14)$$

In the above friction-factor relations, the constant for round tubes can be taken to be  $B = 16$  and  $n = 1$ , respectively, for laminar flow ( $Re_l$  or  $Re_v < 2000$ ), or  $B = 0.079$  and  $n = 0.25$  for turbulent flow ( $Re_l$  or  $Re_v \geq 2000$ ).

Figure 11 shows the comparison of applying the above nucleate and convective terms into time fraction model to predict local heat transfer coefficients and experimental results. The dash lines represent the nucleate and convective boiling terms of the conventional empirical correlations. It is observed that conventional empirical correlations without time fraction model obviously overpredict the experimental results. On the other hand, by introducing Eqns. (6) and (7), a better-predicted result can be obtained. However, since detailed heat transfer characteristics of each flow patterns are still unknown, advanced investigations on these flow patterns are still necessary for more precise predictions.

#### 4. CONCLUSIONS

Visualization of convective boiling flow modes in a microtube with the simultaneous measurement of local heat transfer coefficients was carried out and a concept of building a time-dependent model on heat transfer in microtubes has been proposed. Finally, the following facts can be concluded:

1. The contradiction of dissimilarity in heat transfer characteristics and similarity in pressure loss characteristics between conventional and micro tubes can be explained by the semi-periodic variations of flow patterns observed in microtubes. The decreasing ratio of the bubbly flow pattern with increasing vapor quality in one period leads to the decreasing local heat transfer coefficient with increasing vapor quality. In the mean time, the dominance of plug, slug and annular flow patterns remain similar between conventional and micro tubes.
2. Relatively good predictions of local heat transfer coefficients can be obtained by applying time fraction characteristics to current empirical correlations. However, in order to obtain correct prediction for engineering applications advanced research works considering detailed heat transfer mechanisms in each flow pattern are still needed.
3. As described in the introduction, the heat transfer characteristics of individual flow patterns in microtubes are similar to the corresponding flow patterns in conventional tubes. However, the semi-period variation of the flow patterns leads to the peculiar heat transfer characteristics in convective boiling in microtubes.

#### REFERENCES

- Brereton, G. J., Crilly, R. J., Spears, J. R., 1998. Nucleation in small capillary tubes. Chem. Phys. 230, 253-265.
- Carey, V. P., 1992, Liquid-vapor phase-change phenomena, Hemisphere Publishing Corporation.
- Chen, J. C., 1966, Correlation for Boiling Heat Transfer to Saturated Fluid in Convective Flow. I and EC Process Design and Development 5, 322-329.
- Guerrieri, S. A., and Talty, R. D., 1956, A Study of Heat Transfer to Organic Liquids in Single-Tube Natural Circulation Vertical Tube Boilers. Chem. Eng. Symp. Ser., 52, no. 19, 69-77.
- Hetsroni, G., Mosyak, A., Segal, Z. and Pogrebnyak, E., 2003. Two-phase flow patterns in parallel micro-channels. Int. J. Multiphase Flow 29, 341-360.
- Kandlikar, S. G., 2004. Heat Transfer Mechanisms During Flow Boiling in Microchannels. Trans ASME: J. Heat Transfer 126, 8-16.
- Ravigururajan, T. S., 1998. Impact of channel geometry on two-phase flow heat transfer characteristics of refrigerants in microchannel heat exchangers, Trans ASME: J. Heat Transfer. 120, 485-491.
- REFPROP, 1998. Thermodynamic and transport properties of refrigerants and refrigerant mixtures, NIST standard reference database 23, version 6.01.
- Saitoh, S., Daiguji, H., Hihara, E., 2000. Boiling heat transfer and pressure drop of HFC134a in horizontal

small-diameter tubes. Proc. 39th National Heat Transfer Symp. of Japan, Sapporo, Japan, 667-668.

Serizawa, A., Feng, Z., Kawara, Z., 2002. Two-phase flow in microchannels. Exp. Therm. Fluid Science 26, 703-714.

Steinke, M. E., Kandlikar, S. G., 2003. Flow boiling and pressure drop in microchannels. First International Conference on Microchannels and Minichannels, April 24-25, Rochester, NY, ASME.

Thomas, C. and Chih-Ming, H., 2004. Transport of Bubbles in Square Microchannels. Phys. Fluids. 16, 4575-4585.

Yen, T. -H., Kasagi, N. Suzuki, Y., 2003. Forced Convective Boiling Heat Transfer in Microtubes at Low Mass and Heat Fluxes. Int. J. Multiphase Flow. 29, 1771-1792.

Yen, T. -H., Kasagi, N. Suzuki, Y., 2004. Visualization of convective boiling in a microtube with simultaneous measurement of local heat transfer. Int. Forum on Heat Transfer 2004, November 24-26, Kyoto, Japan, 119-120

#### NOMENCLATURE

$D_i$ : inner diameter of the test section (mm)

$f$ : friction factor

$h$ : heat transfer coefficient (W/m<sup>2</sup>s).

$\dot{m}$ : mass flux

$P_{avg}$ : average pressure in the test section [Pa]

$P_{in}$ : pressure at the test section inlet [Pa]

$P_{sat}$ : saturated pressure [Pa]

$q$ : heat flux

$T_{air}$ : environment temperature [ ]

$T_{ref}$ : refrigerant temperature [ ]

$T_{sat}$ : saturated temperature [ ]

$T_{sup}$ : liquid superheat temperature [ ]

$T_{wout}$ : outer wall temperature [ ]

$T_{win}$ : inner wall temperature [ ]

$t$ : time (sec.)

$\Delta P_{fl}$ : single phase pressure loss [Pa]

$\Delta P_{sub}$ : pressure loss of the subcooled liquid region [Pa]

$\Delta P_{sup}$ : pressure loss of the superheated gas region [Pa]

$\Delta P_{total}$ : total pressure loss in the test section [Pa]

$\Delta T_{sat}$ : temperature difference between the wall and the saturated liquid [K]

$\Delta T_w$ : temperature difference between the wall and the liquid [K]

$\alpha$ : time fraction of each flow pattern in one period

$\chi$ : vapor quality

$\tau$ : period of the flow pattern variation (sec.).